Time-lapse image-domain velocity analysis using adjoint-state methods

Jeffrey Shragge, CPGCO2, The University of Western Australia,*
Tongning Yang and Paul Sava, Center for Wave Phenomena, Colorado School of Mines

SUMMARY

Adjoint-state methods (ASMs) have proven successful for calculating the gradients of the functionals commonly found in geophysical inverse problems. The 3D image-domain formulation of the seismic velocity estimation problem uses imperfections in 3D migrated images to form an objective function, which is minimized using a combined ASM plus line-search approach. While image-domain methods are less sensitive than their data-domain counterparts because they are based largely on wavefield kinematics and not directly matching amplitudes, they are more robust to poorer starting models, which makes them attractive for the early stages of seismic velocity estimation. For time-lapse (4D) seismic scenarios, we show that the 3D ASM approach can be be extended to multiple datasets to offer high-quality estimates of production- and/or injection-induced subsurface change. We discuss two different penalty operators that lead to what we term absolute and relative inversion strategies. The absolute approach straightforwardly uses the difference of two independent 3D inversions to estimate a 4D slowness perturbation. The relative approach directly incorporates the baseline image into the penalty function to highlight where the baseline and monitor images are different and to mask where they are similar - even if reflectors are imperfectly focused. Both these techniques yield good 4D slowness estimates for synthetic data; however, we assert that the relative approach is more robust and preferable to the absolute strategy in the presence of 4D field noise because it represents a less-demanding inversion goal.

INTRODUCTION

Adjoint-state methods (ASMs) have been used with success for a number of years in seismic exploration as an effective approach for calculating the gradient of a functional [see the overviews of Plessix (2006) and Symes (2009)]. While the majority of studies have focused on data-domain applications - in particular full waveform inversion (FWI) (Tarantola, 1984; Pratt, 1999) - a number of authors have explored the complementary image-domain tomography strategy (Girard and Vasconcelos, 2010; Yang and Sava, 2011). This inversion approach, based largely on wavefield kinematics, uses an objective function (OF) derived from observed imperfections in migrated images (i.e., poorly focused subsurface-offset panels). Because image-domain approaches do not formally match field data amplitudes, they afford lower resolution than data-domain methods; however, they are less sensitive to the manifold factors that can affect amplitude (e.g., illumination, anisotropy, etc). While this is usually considered a negative trait one important corollary is that kinematically oriented image-domain ASMs are usually more robust than data-domain approaches because they satisfy less demanding inversion criteria. This leads to an increased likelihood of converging toward the correct - though more bandlimited - inversion result.

The goal of image-domain ASM tomography is to invert for model slowness perturbations, $\Delta s_1 \equiv s_1 - s_0$, that represent the difference between the true and background models, s_1 and s_0, respectively. The key steps of this non-linear inversion approach are similar to data-domain implementations: i) compute the state variables represented by the forward modeled seismic wavefields; ii) calculate the adjoint sources based on the OF and state variables; iii) compute the adjoint state variables represented by the backpropagated adjoint sources; and iv) calculate the gradient estimate by combining the forward and adjoint state variables through an imaging condition. In order to speed up convergence in ASM inversion problems, one normally incorporates a judicious penalty operator that upweights energy located away from zero subsurface offset while excluding that already focused about zero offset. This is often accomplished through use of a differential semblance operator (DSO) (Shen et al., 2005) that, by definition, cancels out a perfectly focused image. ASM-derived model perturbations are useful when used outright for generating a final migration image, but they could also serve as input to a further higher-resolution data-domain velocity inversion analysis (e.g., FWI).

The 4D ASM velocity estimation problem shares many similarities with - and can be viewed as an extension of - the corresponding 3D ASM inversion problem. One key difference is that there are now multiple data sets to work with (i.e., baseline and monitor) as well as multiple slowness perturbations to recover (i.e., the baseline Δs_1, monitor Δs_2, and time-lapse Δs_{TL} differences). Unlike the 3D problem where, by definition, one seeks the *absolute* slowness perturbation that optimally focuses subsurface offset gathers at zero offset, we discuss how the 4D scenario can be solved by implementing one of two strategies. First, one can set up two separate tomographic inversions to independently estimate Δs_1 and Δs_2, and then take their difference to form an *absolute* time-lapse slowness perturbation. Second, one may directly compute a *relative* estimate of the time-lapse slowness difference by appropriately coupling the baseline and monitor datasets in the inversion. We accomplish this through a strategy where baseline image information is introduced into a new penalty function that we apply when inverting the monitor dataset for the $\mathbf{\Delta s_2}$ estimate.

In this abstract we examine the relative 4D approach that uses an image-derived penalty function to upweight energy in the monitor image not spatially coincident with that in the baseline image while downweighting that which is co-located - even if not optimally focused. Thus, this represents a *relative* change between the monitor and baseline image that is analogous to the illumination compensation discussed in Yang et al. (2012). We begin by briefly reviewing the 3D ASM theory and detailing the two 4D extensions. We then present the results of two

inversion experiments that examine the similarities and differences between the absolute and relative 4D ASM approaches.

ADJOINT-STATE METHOD THEORY

Given a one-way frequency-domain wave operator, $\mathscr{L}$, and its adjoint, $\mathscr{L}^\dagger$, we write the 3D forward modeling problem as:

$$\begin{bmatrix} \mathscr{L}(\mathbf{x},\omega,s_0) & 0 \\ 0 & \mathscr{L}^\dagger(\mathbf{x},\omega,s_0) \end{bmatrix} \begin{bmatrix} u_s(\mathbf{e},\mathbf{x},\omega) \\ u_r(\mathbf{e},\mathbf{x},\omega) \end{bmatrix} = \begin{bmatrix} f_s(\mathbf{e},\mathbf{x},\omega) \\ f_r(\mathbf{e},\mathbf{x},\omega) \end{bmatrix} \tag{1}$$

where $\mathbf{x}$ are the spatial coordinates; ω is frequency; s_0 is the background slowness field (formally the square root of model parameters m); u_s and u_r are the computed source and receiver wavefields corresponding to source index $\mathbf{e}$; and f_s and f_r are the source and recorded data. State variables, u_s and u_r, both solutions to the (acoustic) wave equation, are used to formulate an objective function (OF) $\mathscr{H}$ that, for the image-domain ASM tomography problem, is based on minimizing image inconsistencies (i.e., poorly focused subsurface-offset gather) caused by an unknown slowness perturbation Δs_1

$$\mathscr{H} = \frac{1}{2}\,||K_I(\mathbf{x})P(\mathbf{x},\lambda)r(\mathbf{x},\lambda)||^2_{\mathbf{x},\lambda}\,, \tag{2}$$

where $r(\mathbf{x},\lambda)$ is an extended image volume (Sava and Vasconcelos, 2010) formed by cross-correlating the state variables in a direction denoted by λ (herein taken to be horizontal)

$$r(\mathbf{x},\lambda) = \sum_{\mathbf{e},\omega} \overline{u_s(\mathbf{e},\mathbf{x}-\lambda,\omega)}\,u_r(\mathbf{e},\mathbf{x}+\lambda,\omega)\,. \tag{3}$$

Mask operator $K_I(\mathbf{x})$ is used to restrict the OF evaluation to certain image locations, while penalty operator $P(\mathbf{x},\lambda)$ highlights the defocusing in $[\mathbf{x},\lambda]$ hypercube within extended image $r(\mathbf{x},\lambda)$. In the absence of any other information the DSO penalty function, defined by $P(\lambda) = |\lambda|$ and shown in Figure 1(a), has been shown to produce impressive ASM inversion results at a reasonable rate of convergence.

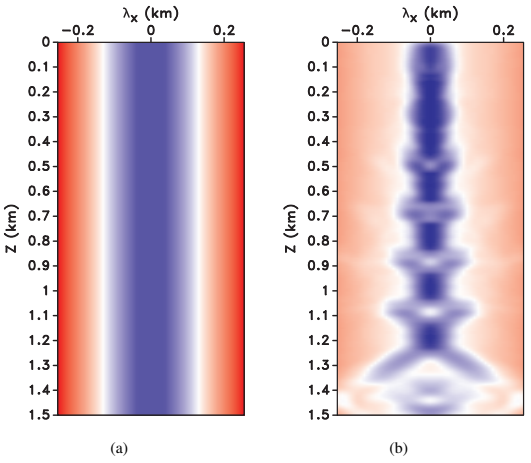

Figure 1: Penalty functions P where the blue-to-red color scheme goes from zero to unity. (a) DSO operator. (b) Weight operator function derived from an existing (baseline) image.

Having defined a penalty function we can specify the adjoint sources, g_s and g_r, used to form the adjoint state variables as the derivatives of $\mathscr{H}$ (equation 2) with respect to state variables u_s and u_r:

$$\begin{bmatrix} g_s(\mathbf{e},\mathbf{x},\omega) \\ g_r(\mathbf{e},\mathbf{x},\omega) \end{bmatrix} = ||K_I(\mathbf{x})||^2 \begin{bmatrix} \sum\limits_{\lambda} ||P(\mathbf{x},\lambda)||^2\,\overline{r(\mathbf{x},\lambda)}\,u_r(\mathbf{e},\mathbf{x}+\lambda,\omega) \\ \sum\limits_{\lambda} ||P(\mathbf{x},\lambda)||^2\,r(\mathbf{x},\lambda)\,u_s(\mathbf{e},\mathbf{x}-\lambda,\omega) \end{bmatrix}. \tag{4}$$

The adjoint-state variables, a_s and a_r, are the wavefields obtained by backward and forward modeling using the corresponding adjoint sources

$$\begin{bmatrix} \mathscr{L}^\dagger(\mathbf{x},\omega,s_0) & 0 \\ 0 & \mathscr{L}(\mathbf{x},\omega,s_0) \end{bmatrix} \begin{bmatrix} a_s(\mathbf{e},\mathbf{x},\omega) \\ a_r(\mathbf{e},\mathbf{x},\omega) \end{bmatrix} = \begin{bmatrix} g_s(\mathbf{e},\mathbf{x},\omega) \\ g_r(\mathbf{e},\mathbf{x},\omega) \end{bmatrix}. \tag{5}$$

The gradient estimate is then formed by correlating the state and adjoint-state variables,

$$\frac{\partial \mathscr{H}}{\partial m} = \sum_{\mathbf{e},\omega} \frac{\partial \mathscr{L}}{\partial m} \left[u_s(\mathbf{e},\mathbf{x},\omega)\overline{a_s(\mathbf{e},\mathbf{x},\omega)} + u_r(\mathbf{e},\mathbf{x},\omega)\overline{a_r(\mathbf{e},\mathbf{x},\omega)} \right]. \tag{6}$$

To find the slowness perturbation estimate, $\Delta s_1^{(i)}$, we use a gradient line-search that minimizes $\mathscr{H}$ at the current n^{th} iteration, which e then use to update model parameters for the n+1th iteration (i.e., $s_1^{(n+1)} = s_0 + \sum\limits_{i=1}^{n} \Delta s_1^{(i)}$). The inversion procedure continues until the convergence criterion is met at the N^{th} iteration and the optimal slowness perturbation estimate $\Delta s_1 = \sum\limits_{n=1}^{N} \Delta s^{(n)}$ found.

As discussed above there are two different strategies to the 4D ASM velocity inversion problem: *independent* and *relative*. In the independent approach one performs separate inversions to obtain independent 3D ASM tomography estimates of the baseline and monitor slowness perturbations from the common s_0 model (i.e., Δs_1 and Δs_2) . The time-lapse estimate is assumed to be their difference: $\Delta s_{TL} \equiv \Delta s_2 - \Delta s_1$. Judicious 4D practice would suggest that one should use the same model weighting function K_I and penalty operator P in the two independent inversion problems; to do otherwise would lead to differently weighted back-projections that could cause an erroneous Δs_{TL} estimate.

The relative 4D approach recognizes that, in fact, there is prior information in the baseline image that can be incorporated directly into a penalty function for monitor inversions. Figure 1(b) presents an example of an image-derived weight that we apply as a penalty function. We use a smoothing operator on the baseline image envelope and then apply a 2D AGC filter to upweight weaker reflectors toward the amplitudes of the stronger ones. While most energy in the resulting panel is focused around $\lambda = 0$, some residual exists away from zero subsurface offset indicating that we used an imperfect migration slowness model. (Figure 1(b) also includes a multiplicative DSO penalty function that provides the observed increased weighting at farther absolute offsets.) Applying this weighting function in the inversion scheme will penalize and largely cancel out energy common to both images - even where it is

equally poorly focused. Accordingly, the only contributions to the time-lapse estimate will be from the *relative* changes between the images. Importantly for 4D practice, this approach does not rely on baseline/monitor data or image difference volumes that are notoriously noisy due to non-repeatable 4D acquisition. As such, we assert that this approach (where required) is likely to be more robust than other 4D velocity inversion approaches that involve computing data differences.

EXPERIMENT

Our numerical experiment tests the validity of the two 4D inversion approaches in a relatively noise-free environment. Figure 2(a) presents the baseline slowness perturbation Δs_1 from a constant background model, while Figure 2(b) presents the baseline and monitor perturbations together, $\Delta s_1 + \Delta s_2$. (We plot these slowness panels and those that follow at the same color scale and will henceforth omit the scale bar.) Using a elastic finite difference modeling operator we generated baseline and monitor datasets, f_{r_1} and f_{r_2}, using the slowness models shown in Figure 2, a shear-wave slowness profile $s\sqrt{3}$, and a density profile comprised of six equally space horizontal reflectors running the full model width.

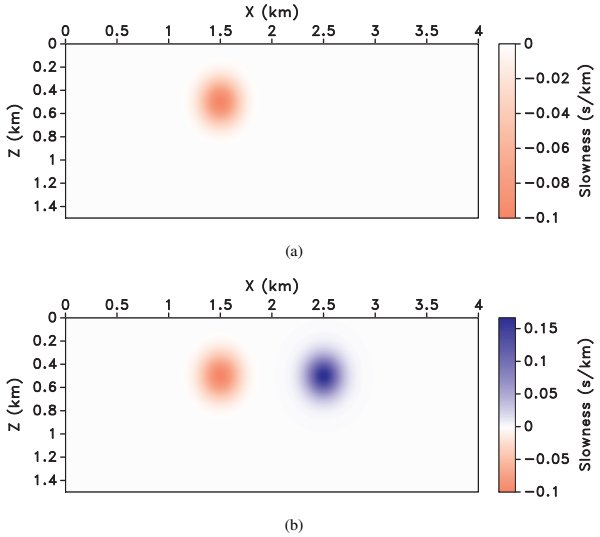

Figure 2: Slowness perturbations from a constant s_0=0.5 s/km background slowness model used in the synthetic tests. (a) Baseline perturbation Δs_1. (b) Baseline plus monitor perturbations $\Delta s_1 + \Delta s_2$.

Figure 3(a) presents the one-way wave-equation migration image of the baseline dataset using $s_0 = 0.5$ s/km as the migration slowness model. The reflectors are imaged horizontal except near the location of the baseline perturbation at $x = 1.5$ km. We applied 15 iterations of image-domain ASM tomography inversion scheme discussed above to generate the Δs_1 slowness perturbation estimate shown in Figure 3(b). Figure 3(c) presents the baseline image remigrated with slowness model $s_0 + \Delta s_1$. We note that the baseline slowness estimate is a good approximation of the true perturbation in Figure 2(a)and has done a decent job of flattening the six reflectors.

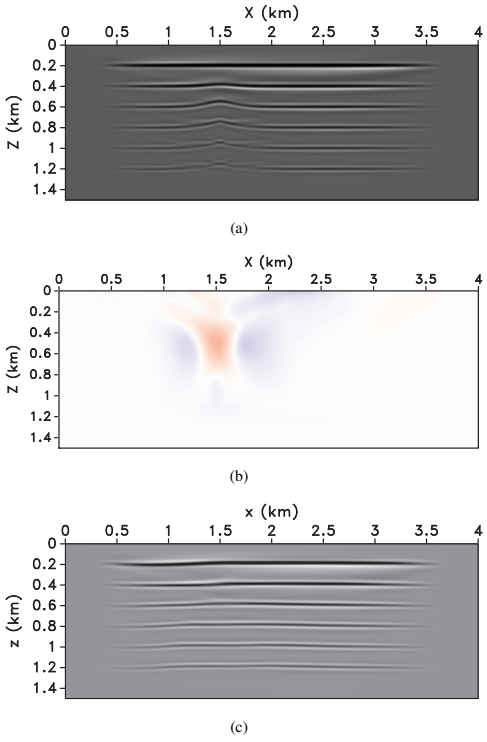

Figure 3: Baseline inversion experiment. (a) Baseline image generated using $s_0 = 0.5$ s/km. (b) Inverted baseline perturbation Δs_1. (c) Baseline image using $s_0 + \Delta s_1$.

Figure 4(a) shows the migrated monitor image constructed from the estimated baseline model $s_0 + \Delta s_1$. The imaged reflectors are again nearly horizontal save for the pull down centered about $x = 2.5$ km as expected from the introduced monitor slowness perturbation in Figure 2(b). Figure 4(b) and 4(c) presents a horizontal concatenation of a subset of the penalized image offset gathers corresponding to the image in Figure 4(a). Figure 4(b) shows the effect of applying the DSO-only penalty function from Figure 1(a). We observe that while the majority of residual energy is located in the vicinity of where the monitor slowness perturbation occurs, some unflattened energy remains between $x = 0.5$ km and $x = 2.0$ km due to the imperfect baseline velocity analysis. In general, this suggests that using the DSO penalty alone for 4D velocity analysis can lead to contaminated estimates of Δs_{TL} because residual energy from the baseline analysis can leak into the monitor inversion.

Figure 4(c) presents the monitor image residuals after applying the combined DSO+4D penalty, an example panel of which is shown in Figure 1(b). Here, the consistency in the migrated baseline and monitor images - as encapsulated in the 4D penalty operator - effectively masks most-to-all of the residual energy occurring between $x = 0.5$ km and $x = 2.0$ km. The remaining energy residuals are now more closely associated with those directly stemming from the monitor perturbation, and are likely to give an equal or better result than when following the

DSO-only approach.

Figure 5(a) presents the $\Delta s_{TL} \equiv \Delta s_2 - \Delta s_1$ time-lapse slowness estimate from the independent strategy, while Figure 5(b) shows that of the relative approach. We observe that having the more restricted energy residuals using the 4D+DSO penalty function helps to spatially localize the imaged perturbation. We also observe in Figure 5(a) that the ASM inversion is still trying to image the baseline perturbation that was not completely accounted for in the first stage of analysis. As discussed above this represents "inversion leakage" between the baseline and monitor surveys and could possible introduce erroneous interpretation in more realistic tests.

CONCLUSIONS

We present an extension of 3D adjoint-state methods in the image domain to the 4D seismic velocity inversion problem. We discuss different absolute and relative inversion strategies that use different penalty functions to down- and upweight different components of imaged wavefield energy. The independent 4D inversion approach uses the difference between two separate 3D inversion estimates to compute the 4D perturbation. The relative inversion strategy couples the baseline and monitor datasets together by incorporating the baseline image directly into the penalty operator. This allows monitor image energy matching that in the baseline image - but itself not necessarily optimally focused - to be masked and precluded from inversion. We assert that the masking strategy should make ASM velocity inversion more robust in the present of 4D field data noise such as non-repeatable acquisition.

ACKNOWLEDGMENTS

We thank David Lumley for helpful discussions. Shragge acknowledges WAERA support through a Research Fellowship. This research was partly funded by the sponsors of the UWA:RM consortium. Simulation results were computed using IVEC HPC facilities. The reproducible numerical examples use the Madagascar open-source package (http://www.reproducibility.org).

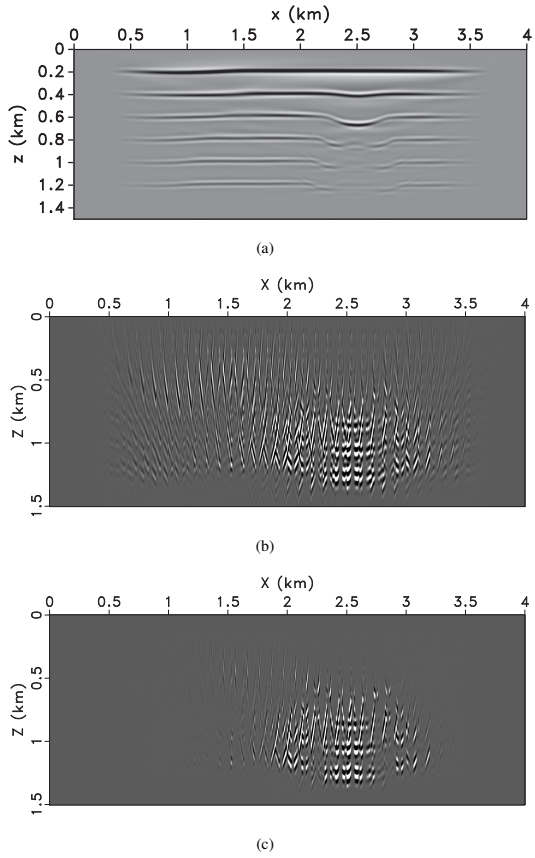

Figure 4: Monitor inversion experiment. (a) Image generated using estimated slowness field $s_0 + \Delta s_1$. (b) Horizontal concatenation of penalized subsurface offset gathers for th monitor survey data for DSO penalty operator. (c) As in (b) but for 4D+DSO penalty operator.

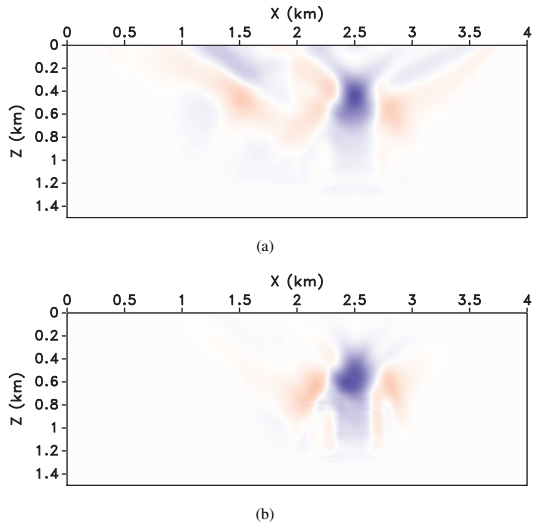

Figure 5: Monitor inversion results. (a) Absolute 4D strategy perturbation estimate Δs_2. (b) Relative 4D strategy perturbation estimate Δs_2..

REFERENCES

Girard, A., and I. Vasconcelos, 2010, Image-domain time-lapse inversion with extended images: SEG Expanded Abstracts, 29, Soc. of Expl. Geophys., 4200–4203.

Plessix, R.-E., 2006, A review of adjoint state method for computing the gradient of a functional with geophysical applications: Geophysical Journal International, **167**, 495–503.

Pratt, R. G., 1999, Seismic waveform inversion in the frequency domain, part 1: Theory and verification in a physical scale model: Geophysics, **64**, 888–901.

Sava, P., and I. Vasconcelos, 2010, Extended imaging conditions for wave-equation migration: Geophysical Prospecting, **59**, 35–55.

Shen, P., W. Symes, S. Morton, and H. Calandra, 2005, Differential semblance velocity analysis via shot profile migration: SEG Expanded Abstracts, 24, Soc. of Expl. Geophys., 2249–2252.

Symes, W., 2009, Migration velocity analysis and waveform inversion: Geophysical Prospecting, **56**, 765–790.

Tarantola, A., 1984, Inversion of seismic reflection data in the acoustic approximation: Geophysics, **49**, 1259–1266.

Yang, T., and P. Sava, 2011, Image-domain waveform tomography with two-way wave-equation: SEG Expanded Abstracts 30, Soc. of Expl. Geophys., 2591–2596.

Yang, T., J. Shragge, and P. Sava, 2012, Illumination compensation for image-domain wavefield tomography: Presented at the Proceedings of the 74th Annual International Meeting, European Association of Geoscientists and Engineers.